Insight into the Thermodynamic Structure of Blowing-Snow Layers in Antarctica from Dropsonde and *CALIPSO* Measurements

STEPHEN P. PALM

Science Systems and Applications, Inc., Lanham, Maryland

YUEKUI YANG

NASA Goddard Space Flight Center, Greenbelt, Maryland

VINAY KAYETHA

Science Systems and Applications, Inc., Lanham, Maryland

JULIEN P. NICOLAS

Byrd Polar and Climate Research Center, The Ohio State University, Columbus, Ohio

(Manuscript received 23 March 2018, in final form 4 October 2018)

ABSTRACT

Blowing snow is a frequent and widespread phenomenon over most of Antarctica. The transport and sublimation of blowing snow are important for the mass balance of the Antarctic ice sheet, and the latter is a major contributor to the hydrological cycle in high-latitude regions. Although much is known about blowing snow from surface observations, knowledge of the thermodynamic structure of deep (>50 m) blowing-snow layers is lacking. Here, dropsonde measurements are used to investigate the temperature, moisture, and wind structure of deep blowing-snow layers over Antarctica. The temperature lapse rate within the blowing-snow layer is at times close to dry adiabatic and is on average between dry and moist adiabatic. Initiation of blowing snow causes the surface temperature to increase to a degree proportional to the depth of the blowing-snow layer. The relative humidity with respect to ice is generally largest near the surface (but less than 100%) and decreases with height, reaching a minimum near the top of the layer. These findings are at odds with the generally accepted theory that blowing-snow sublimation will cool and eventually saturate the layer. The observations support the conclusion that high levels of wind-shear-induced turbulence cause mixing and entrainment of warmer air from above the blowing-snow layer, which suppresses humidity and produces the observed well-mixed temperature structure within the layer. The results may have important consequences for understanding the mass balance of the Antarctic ice sheet and the moisture budget of the atmosphere in high latitudes.

1. Introduction

Snow lifted from the surface and carried aloft by wind and turbulence is known as drifting and blowing snow. Drifting snow is generally defined as airborne snow confined to a maximum height of 2 m. Once snow particles attain a height of greater than 2 m, they are considered to be blowing snow. In high latitudes, blowing snow is important to the atmospheric water budget through sublimation (Tabler 1975; Déry et al. 1998; Frezzotti et al. 2013). In Antarctica, blowing snow is important as part of the ice sheet's mass balance through both sublimation and transport (Lenaerts et al. 2012; Gallée et al. 2001; Palm et al. 2017; Scarchilli et al. 2010). In East Antarctica, blowing snow occurs as frequently as 70% of the time over large areas in winter, averages about 150 m in depth, and can reach heights of 500 m or more (Palm et al. 2011; Mahesh et al. 2003). Because of the scarcity of observations in Antarctica, almost all of what is known about the thermodynamic

Supplemental information related to this paper is available at the Journals Online website: https://doi.org/10.1175/JAMC-D-18-0082.s1.

Corresponding author: Stephen Palm, stephen.p.palm@nasa.gov

DOI: 10.1175/JAMC-D-18-0082.1

structure of deep (>50 m) blowing-snow layers comes from models. Other than at Dome C since 2006 and at the South Pole, there are no routine upper-air observations over the interior of Antarctica, and all other radiosonde stations are located near the coast. In addition, when large blowing-snow storms occur, the conditions are so harsh that they often preclude the launching of radiosondes. Therefore, actual temperature, moisture, and wind observations through the depth of blowing-snow layers are rare or nonexistent.

It is well known that, in general, the temperature structure in the lowest few hundred meters over Antarctica is dominated by a strong inversion caused by radiative cooling, especially in winter (Phillpot and Zillman 1970). The magnitude of the inversion can be related to the surface wind speed, with the strongest inversions occurring in calm or light wind conditions. In some cases, inversion strengths can be as great as 30°C (Wang et al. 2013; Boylan et al. 2016). In the katabatic wind regime, strong winds (and wind shear) at and near the surface can cause turbulent mixing (King and Turner 1997) and an increase in downward turbulent sensible heat flux that causes the surface temperature to rise and a more neutral temperature lapse rate near the ground (Bromwich 1989; Ohata et al. 1985). In addition, the downslope trajectory of katabatic flow warms and dries the air, which can enhance sublimation of falling snow (Grazioli et al. 2017). Most blowing-snow episodes in Antarctica occur in the presence of strong (usually but not always) katabatic winds. Thus, it may be possible that during blowing snow the temperature inversion near the surface is eroded and the air remains below saturation; there are no published measurements that can verify this possibility, however.

Some prior research has suggested that once blowing snow becomes established, the presence of snow particles in the air will tend to have a stabilizing effect that can also damp turbulence (Wamser and Lykossov 1995; Bintanja 1998, 2000). This is caused by the energy required to keep snow particles in suspension at a certain average height above the surface, as the residual upward turbulent stress exerted on the particles must balance the downward force of gravitation. Kodama et al. (1985) discussed the potential influence of blowing snow on the dynamics of Antarctic katabatic winds. They noted that the presence of blowing-snow particles in the airstream causes an increase in the fluid density, thus increasing the katabatic force. Furthermore, the sublimation of snow absorbs heat and is responsible for an additional cooling and an increase in air density. They also mentioned that the transfer of kinetic energy from the air near the surface to blowing-snow particles slows down the katabatic airstream, but they concluded that such a process had a negligible influence.

There are very few measurements of the average boundary layer moisture structure over the interior of Antarctica, especially in winter. Radiosonde observations at Dome C in late autumn (May of 2005) show that in the lowest 200 m, the relative humidity increases with height, reaching a peak of about 80%, and then remains constant to 400 m altitude, at which point it falls abruptly to about 50% (Tomasi et al. 2006). However, these measurements were made in the absence of blowing snow. Most prior research has suggested that once blowing snow is established, sublimation of the airborne snow particles will gradually increase the average relative humidity of the layer, which will ultimately reduce or entirely curtail further sublimation. In essence, blowing-snow sublimation is thought to be a self-limiting process (Mann et al. 2000; Bintanja 2001). However, this assertion has never been proven by the measurement of the humidity profile through the entire extent of deep (50 m or more) blowing-snow layers. All measurements to date, which show that blowing snow will eventually saturate or nearly saturate the air, have been made at or near the surface (Takahashi 1985; Mann et al. 2000). Likewise, models of blowing snow also indicate that the blowing-snow layer quickly saturates and sublimation reduces to near zero in a matter of hours after initiation (Bintanja 2000; Déry and Yau 1999). Models also predict that the surface temperature will decrease during blowing snow as a result of the cooling effect of sublimation (Bintanja 2000).

In this paper we present the first (to our knowledge) profiles of temperature, moisture, and wind through deep blowing-snow layers in an attempt to better understand the processes occurring within the layer and how well they fit with the generally accepted view outlined above. The paper is organized into six sections. Section 2 will present a hypothesis on the possible effects of mixing and entrainment on the observed thermodynamic structure of blowing-snow layers, and section 3 will briefly describe the data and methods used in this paper. In section 4, we present five case studies of dropsondes that fell through blowing-snow layers to examine their temperature, moisture, and wind structure. Section 5 will discuss the results, and we give concluding remarks and a summary in section 6.

2. The effects of turbulent mixing and entrainment

The processes that govern the thermodynamic structure of blowing-snow layers described in section 1 may be partially flawed or incomplete, which could have important consequences. For instance, if deep blowing-snow layers remain unsaturated because of processes like turbulent mixing; entrainment of warmer, less humid air

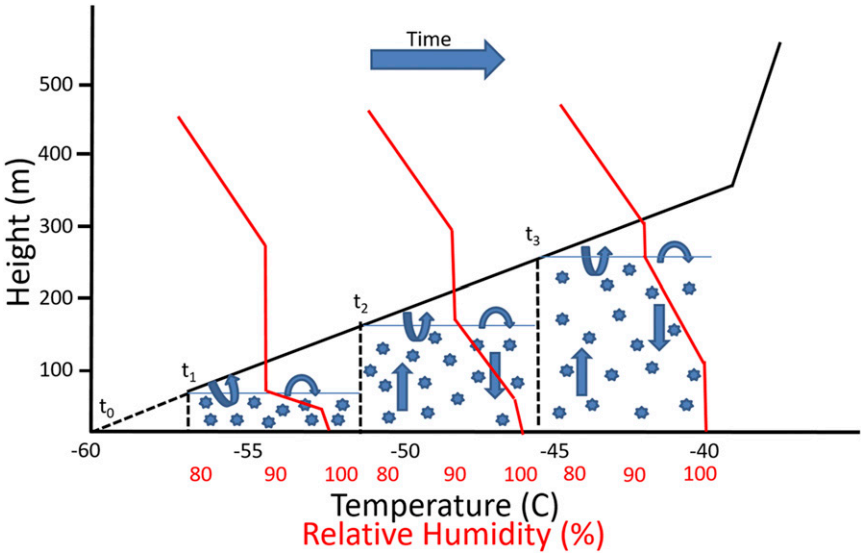

FIG. 1. Conceptual model of the evolution of the temperature (black) and humidity (red) structure as a function of time during a blowing-snow episode.

from above; or downslope warming, it could have a large impact on total layer sublimation, which current atmospheric models are not including. Such moisture-reducing processes were found to be potentially significant in the modeling work of Bintanja (2001). This would then have implications that may further our knowledge of the atmospheric moisture budget and the mass balance of the Antarctic ice sheet.

If blowing-snow sublimation does not completely saturate the entire blowing-snow layer, then what mechanisms must be in play to keep the layer subsaturated? One such process is the potentially large effect of turbulence-induced entrainment on the temperature and moisture structure within the blowing-snow layer. Let us assume that initially, before blowing snow commences, the temperature structure in the lower 300–400 m is one of a strong inversion that extends to the surface (Fig. 1, time t_0). This is typical in calm or light wind conditions in wintertime over most of Antarctica. As wind speed increases and blowing snow is initiated, turbulent mixing ensues and begins to entrain and mix air from above the inversion into the blowing-snow layer. The warmer air mixing downward into the blowing-snow layer will raise the surface temperature, and the temperature profile within the blowing-snow layer will tend to become more isothermal or even near adiabatic due to the turbulent mixing (Fig. 1, time t_1). If wind speed and wind shear continue to increase, and synoptic-scale subsidence is not too great, the blowing-snow layer depth will increase with time and the temperature profile will remain quasi-isothermal through the depth of the layer (black solid and dashed lines in Fig. 1, for times t_2 and t_3). The amount of surface (and blowing-snow layer) temperature increase is related to the depth of the blowing-snow layer (as shown in Fig. 1). This process does not necessarily depend on the presence of blowing-snow particles, but it does depend on wind-shear-induced turbulent mixing and entrainment. However, it is known that blowing-snow particles will increase absorption of longwave radiation, which would also help to warm the layer and increase the temperature at the surface (Yang et al. 2014). This scenario is consistent with the tower and radiosonde observations from Mizuho Station, East Antarctica, that were presented in Ohata et al. (1985). They showed that high wind speed in the katabatic flow will induce turbulent mixing and erode a previously established surface-based inversion, producing a quasi-isothermal temperature profile in the first 50–100 m above the surface. Although not mentioned in that paper, it is possible or even likely that blowing snow was present, given that the surface wind speed for that case was 15–20 m s^{-1}.

The wind-shear-induced turbulent mixing can also have an effect on the relative humidity profile within the blowing-snow layer (red profiles in Fig. 1). The mixing of warmer air down into the blowing-snow layer has the potential to lower the relative humidity and keep it below the saturation point even in the presence of blowing-snow sublimation, at least in the upper portion of the layer (Fig. 1 at times t_1 and t_2). The amount of humidity suppression would depend both on the magnitude of entrainment and mixing and on the gradient of moisture at and immediately above the inversion. Under this scenario, the moisture profile would be near saturation

close to the surface and would tend to decrease with height, but as a whole it would remain below saturation through most of the depth of the blowing-snow layer (Fig. 1, time t_3). Assuming that the air is not saturated, sublimation of blowing-snow particles will tend to cool and moisten the layer. If entrainment of warmer air from above the layer is not sufficient to keep the air from saturating, eventually the sublimation will cease. While the above hypothesis is purely speculative, it is the goal of this paper to use the first documented measurements of temperature, wind, and moisture through deep blowing-snow layers to examine its plausibility.

3. Data and methods

a. *Dropsonde data*

The Concordiasi project, which occurred in the austral autumn of 2010 (from 28 September to 8 December), utilized multiple high-altitude, long-duration balloons to launch 648 dropsondes over Antarctica and surrounding sea ice (Rabier et al. 2010, 2013; Boylan et al. 2016). The dropsondes used the same sensor module as the Vaisala, Inc., RS92 radiosonde and provided profiles of pressure, temperature, relative humidity, and wind speed (using GPS position data) from ~60 hPa to the surface. The descent rate of the dropsondes provides a measurement resolution that varies from a vertical spacing of 5 m near the surface to 30 m at 100 hPa. Given the large number of dropsonde launches and the fact that in late September and October blowing-snow frequency is still very high (Palm et al. 2018), the likelihood of a few dropsondes falling through well-developed blowing-snow layers is very good. We performed an extensive analysis of the times and positions of the dropsondes and identified 28 dropsondes that fell through, or very near to, blowing-snow layers, as identified by the satellite lidar remote sensing technique discussed in Palm et al. (2011, 2017). Nearly all of these cases showed similar temperature and moisture structure, as is shown in the five cases documented here.

The dropsondes used in the Concordiasi project are from the National Center for Atmospheric Research (NCAR) and utilize the Vaisala RS92 sensor. The RS92 temperature sensor has been found to be accurate to better than 0.3°C from the surface to 100 hPa (Nash et al. 2011; Vaisala 2013). The accuracy of the RS92 moisture sensor was thoroughly examined by Miloshevich et al. (2006). In very cold conditions the sensor has a known dry bias that has been corrected in the version-2 data that are used here (see information at https://data.eol.ucar.edu/dataset/221.002). Also very important is the consideration of the lag time of the moisture sensor. Unlike the temperature sensor, the moisture sensor has a considerable response (or lag) time that produces error in the relative humidity measurement. The magnitude of the error is related to the fall speed of the sensor, ambient air temperature, and the rate of change of relative humidity with height. Here we have employed the lag-time correction procedure detailed in Miloshevich et al. (2004). Even with these corrections, it is important to note that the relative humidity derived from the sensor in very cold conditions can still have considerable error. Miloshevich et al. (2006) estimate the moisture sensor accuracy to be about −6% (a dry bias of 6%) for temperatures between −50° and −20°C. Miloshevich et al. (2009) compared RS92 moisture measurements with those of a frost-point hygrometer through a temperature range reaching −70°C. They found that the RS92 relative humidity had a negative bias of approximately 5%–6% at a temperature of −40°C and between 10% and 15% at −70°C. With the exception of one case, the case studies shown here have near-surface temperatures in the range from −55° to −40°C. From the work of Miloshevich et al. (2006, 2009), we estimate the relative humidity data presented here to have a potential negative (dry) bias of approximately 10%–15%.

The relative humidity reported by the dropsonde is with respect to water and must be converted to being with respect to ice. We follow Rogers and Yau (1989) to compute the ratio of the saturation vapor pressure with respect to water to that with respect to ice at ambient temperature T (K):

$$\frac{e_s(T)}{e_i(T)} = \exp\left[\frac{(L_s - L)}{R_v T_0}\left(\frac{T_0}{T} - 1\right)\right], \tag{1}$$

where L_s is the latent heat of sublimation of water, L the latent heat of vaporization, and T_0 is taken to be 273.15 K. The relative humidity measured by the dropsonde is then multiplied by Eq. (1) to convert it to relative humidity with respect to ice. This factor is generally about 1.3–1.4 for temperatures between −40° and −50°C. This conversion is done first, and then the time-lag correction as per Miloshevich et al. (2004) is applied to the resulting humidity profile.

b. CALIPSO *data*

In this paper we use the level-1B calibrated attenuated backscatter data (V4-00) from the Cloud–Aerosol Lidar with Orthogonal Polarization (CALIOP) aboard the *Cloud–Aerosol Lidar and Infrared Pathfinder Satellite Observations* (*CALIPSO*) satellite (Winker et al. 2009). *CALIPSO* was launched in April of 2006 and has been operating continuously (with a few minor data gaps) since June of 2006. Because of the orbit of *CALIPSO*, the data

over Antarctica are confined to north of 82°S and the detection of blowing snow is limited to layers of 30 m or greater in thickness since the vertical resolution of the CALIOP data is 30 m in the lower troposphere. Here we use the algorithm described in Palm et al. (2011, 2017) to detect blowing snow using the CALIOP data.

c. *ERA-5 reanalysis data*

To compare with the dropsonde data near the surface and obtain a broader spatial view of surface conditions in Antarctica during each case study, we used analysis fields (2-m temperature, 2-m relative humidity, and 10-m wind vectors) from the ERA-5 reanalysis recently released by the European Centre for Medium-Range Weather Forecasts (Hersbach and Dee 2016). ERA-5 features a number of improvements upon its predecessor, ERA-Interim, including higher horizontal model resolution (31 vs 80 km) and more vertical levels (137 vs 60 levels). Still, one must keep in mind that ERA-5 does not explicitly resolve blowing-snow processes nor has the vertical model resolution needed to capture the vertical structure of temperature and moisture through the depth of the blowing-snow layers presented here. Note also that, to the best of our knowledge, the dropsonde data are not assimilated by the ERA-5 reanalysis.

d. *AWS data*

Automatic weather stations (AWS) have been operating as an international project in Antarctica since 1980. Today there are approximately 100 AWS in operation, many of which (59) are maintained and operated by the University of Wisconsin. The AWS stations measure air temperature, wind speed, and wind direction at a nominal height of 3 m above the surface and air pressure at the height of the electronics enclosure. Some AWS units measure relative humidity at 3 m and air temperature difference between 3 and 0.5 m above the surface (Stearns and Wendler 1988). The temperature sensor has a resolution of 0.125°C and accuracy of ±0.5°C through the temperature range from +15° to −85°C. The AWS employ a Vaisala HMP-35A humidity sensor with an accuracy of ±5.0% at temperatures down to −55°C. The wind speed measurements have an accuracy of $\pm 0.5\,\mathrm{m\,s^{-1}}$. AWS measurements are routinely ingested into global reanalysis models like ERA-5.

4. Dropsonde and blowing-snow case studies

In this section, we examine the dropsonde data that were serendipitously acquired as the dropsondes fell through blowing-snow layers over Antarctica. As mentioned in the introduction there were 28 such cases found over various areas of the continent. Here we present those where the *CALIPSO* blowing-snow retrieval is closest in space and time to that of the dropsonde. There were no exact coincidences between the dropsondes and the *CALIPSO* observation, but a few are very close in space (<10 km) or time (<30 min). We also tried to choose the cases from different regions of Antarctica so that varying properties like surface slope, elevation, surface temperature, and relative humidity could be sampled. The times and dates of the five cases, the location and times of the dropsondes, and other information are given in Table 1. The dropsonde locations are also shown on the map in Fig. 2, as are the *CALIPSO* tracks and locations of the AWS discussed in the text.

For each case we have also prepared Figs. S1–S4 in the online supplemental material that show the ERA-5 reanalysis 2-m temperature, relative humidity with respect to ice and 10-m wind speed for each of the five case studies. In these figures, the plus signs mark the approximate location of the dropsonde for each case.

a. *Case I*

On 12 October 2010, a large blowing-snow storm was occurring over most of Wilkes Land, Antarctica. An analysis of CALIOP and MODIS data over the period 8–14 October 2010 showed that the storm began late in the day on 9 October 2010 and continued for 3–4 days. The false-color MODIS image shown in Fig. 3 illustrates the large area covered by this storm at 0550 UTC 12 October 2010. In this image, the snow- and ice-covered surface is blue, while clouds are a bright white. Blowing snow is indicated by the grayish-white areas that cover most of the region west of approximately 155°E. The apparent opacity or darkness of these areas is related to the optical depth of the blowing-snow layer. The Antarctic coastline is indicated by the green dots in the figure. In Fig. 3 the portions of the *CALIPSO* tracks on 12 October 2010 for which blowing snow was detected are depicted by the yellow lines. Note that some portion of all *CALIPSO* tracks over this area on 12 October 2010 indicated the presence of blowing snow. The positions of the two dropsondes that were launched in this region and on the same day (our cases I and II) are shown in Fig. 3 by the small solid green boxes.

Figure 4 shows the CALIOP 532-nm attenuated backscatter and the dropsonde temperature, relative humidity (with respect to ice), and wind profiles for all five cases. Figure 4a (case I) shows the CALIOP attenuated backscatter data acquired at 0553 UTC 12 October 2010. The blowing-snow layer corresponds to the higher CALIOP backscatter (mostly green and purple colors) that averages between 100 and 200 m thick (the backscatter-magnitude color bar is shown in Fig. 4d). To the right of the CALIOP backscatter image are

TABLE 1. Dropsonde date, location, and time and the time, distance, and elevation of the *CALIPSO* track nearest the dropsonde for the five case studies.

			Nearest *CALIPSO* track		
	Date	Dropsonde location and time	Distance from dropsonde	Time	Begin/end elev (m MSL)
Case I	12 Oct 2010	71.61°S, 143.44°E; 1242 UTC	5 km	0553 UTC	2400/2220
Case II	12 Oct 2010	77.19°S, 121.09°E; 1049 UTC	150 km	0730 UTC	2490/3150
			200 km	0908 UTC	2850/3360
Case III	30 Oct 2010	81.07°S, 50.54°E; 1756 UTC	50 km	1530 UTC	3690/3510
Case IV	2 Oct 2010	79.47°S, 105.73°W; 0750 UTC	40 km	0510 UTC	1800/1500
Case V	1 Nov 2010	80.03°S, 175.84°E; 0959 UTC	12 km	1020 UTC	20/20

temperature (black line with scale at the bottom of the figure) and relative humidity profiles (red line, with respect to ice, with scale at top) from a dropsonde launched at 1242 UTC the same day. The location of the profile is indicated by the asterisk and the "I" drawn on the map (Fig. 2) and came within just 5 km of the *CALIPSO* track. The position of minimum separation between the dropsonde and the *CALIPSO* track is indicated by the vertical yellow arrow drawn at the top of the image. The height scale to the left of the image is with respect to mean sea level (MSL) at the location of the dropsonde (the surface elevation of which is 2200 m). The change in surface elevation along the *CALIPSO* track has been removed in the backscatter image shown. However, note that Fig. 2 includes surface elevation contours from which the change in elevation along the *CALIPSO* track can be deduced. In addition, Table 1 lists the beginning and ending elevation of all *CALIPSO* tracks. In Figs. 5–7 we also display the dropsonde data for the five cases, but with a smaller height and temperature/humidity range so that more detail can be discerned in the temperature and moisture structure within the blowing-snow layer. We will refer to them when discussing the thermodynamic structure of the blowing-snow layer below.

Although in case I the dropsonde came within a few kilometers of the *CALIPSO* track, the dropsonde data were acquired about 7 h after the CALIOP backscatter data. We are confident that blowing snow was still present at the time and location of the dropsonde

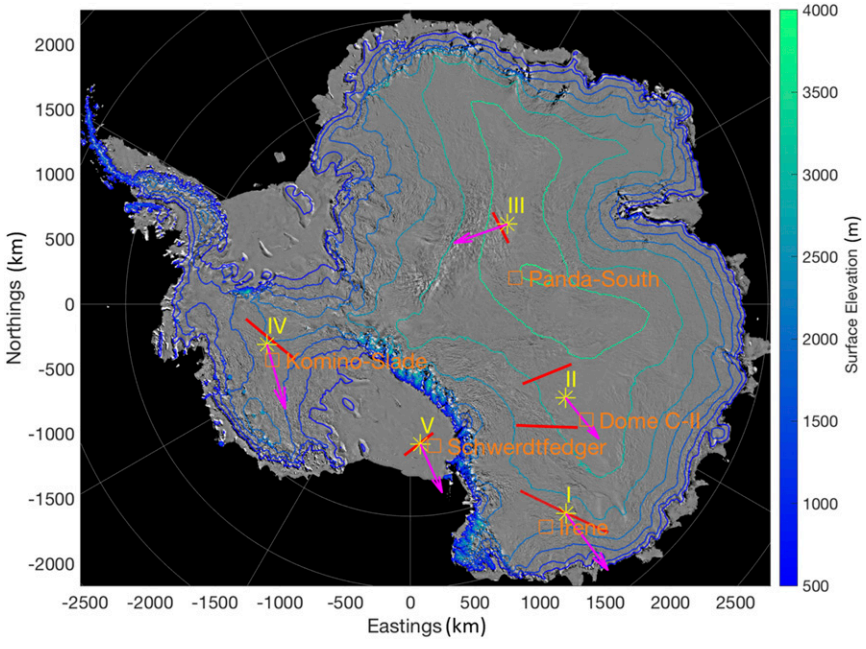

FIG. 2. Map of Antarctica showing surface elevation contours, the locations of the dropsondes (yellow asterisks), *CALIPSO* tracks (red), and AWS stations (orange boxes) for the five case studies. The elevation contours are color coded, with the elevation color bar shown on the right. Also shown is the 50-m (above the surface) wind vector as obtained from the dropsonde data (pink arrows).

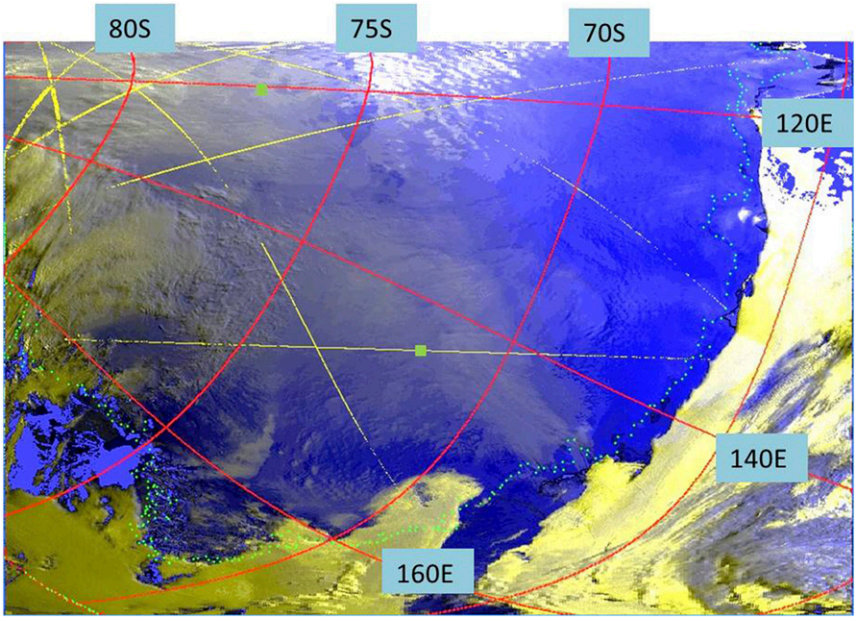

FIG. 3. MODIS false-color image at 0550 UTC 12 Oct 2010.

because it was also detected in this area from a *CALIPSO* pass that occurred at 1400 UTC (2 h after the dropsonde time) and about 200 km to the east of the dropsonde location. At that time and location, the blowing-snow layer was about 150 m deep and thus was somewhat shallower than that shown in Fig. 4a. Also, MODIS observations the following day (13 October 2010) at 0640 UTC showed blowing snow continuing in this general area. It is often true that blowing-snow storms persist for days over large regions in Antarctica (Palm et al. 2011). The temperature profile in Figs. 4a and 5a shows the normal low-level inversion beginning at about 350 m above the surface or 2340 m MSL. However, it does not continue to the surface but rather, at the height of the top of the blowing-snow layer (~140–150 m above the surface), the temperature profile increases as it descends. The average lapse rate in the lowest 150 m is almost dry adiabatic (−0.0088° vs −0.0098°C m^{-1}), which is between moist and dry adiabatic. There are even regions of the temperature profile that have a lapse rate less than dry adiabatic (Fig. 5a, between 20 and 50 m above the surface). Without knowing that this temperature profile was acquired over Antarctica in late winter/early spring during nighttime, one would suspect that it was taken through a shallow convective layer. In the lowest 150 m it is not at all typical of the usual Antarctic temperature profile. Note also that, if the inversion were to continue to the ground, the surface temperature would be about 5°–10°C lower than what is measured (−50°C).

The relative humidity profile in Figs. 4a and 5a shows ample structure both above and within the blowing-snow layer. Well above the blowing-snow layer, the relative humidity averages about 75%. As the dropsonde descends into the blowing-snow layer, and at almost the exact height of the inflection point of the temperature profile (~140 m above the surface), the relative humidity begins to increase from a value of about 60% near the top of the layer to about 82% within roughly 10–20 m of the surface. From there it decreases to a value of about 75% at the surface. Note that the observed temperature profile shown in Fig. 5a is consistent with a layer that is on average not saturated (average lapse rate greater than moist adiabatic).

The wind speed (blue line in Fig. 4a with scale at bottom and black line in Fig. 5b) reaches a maximum of almost 24 m s^{-1} at an altitude of about 2350 m, which is 150 m above the surface and very near the top of the blowing-snow layer. From that altitude the wind speed decreases linearly to roughly 15 m s^{-1} close to the surface. The wind direction (green line with scale at top and red line in Fig. 5b) varies from about 155° at 2400 m altitude to 184° at 50 m above the surface. The magnitude of the wind speed and directional shear in the lower 200 m (corresponding to the blowing-snow layer) will undoubtedly produce turbulence in the layer and promote mixing. It is apparent that the mixing has destroyed the temperature inversion at the surface (assuming it existed prior to the onset of high wind speeds and blowing snow) by the process of entrainment of warmer air from above and or adiabatic warming of the

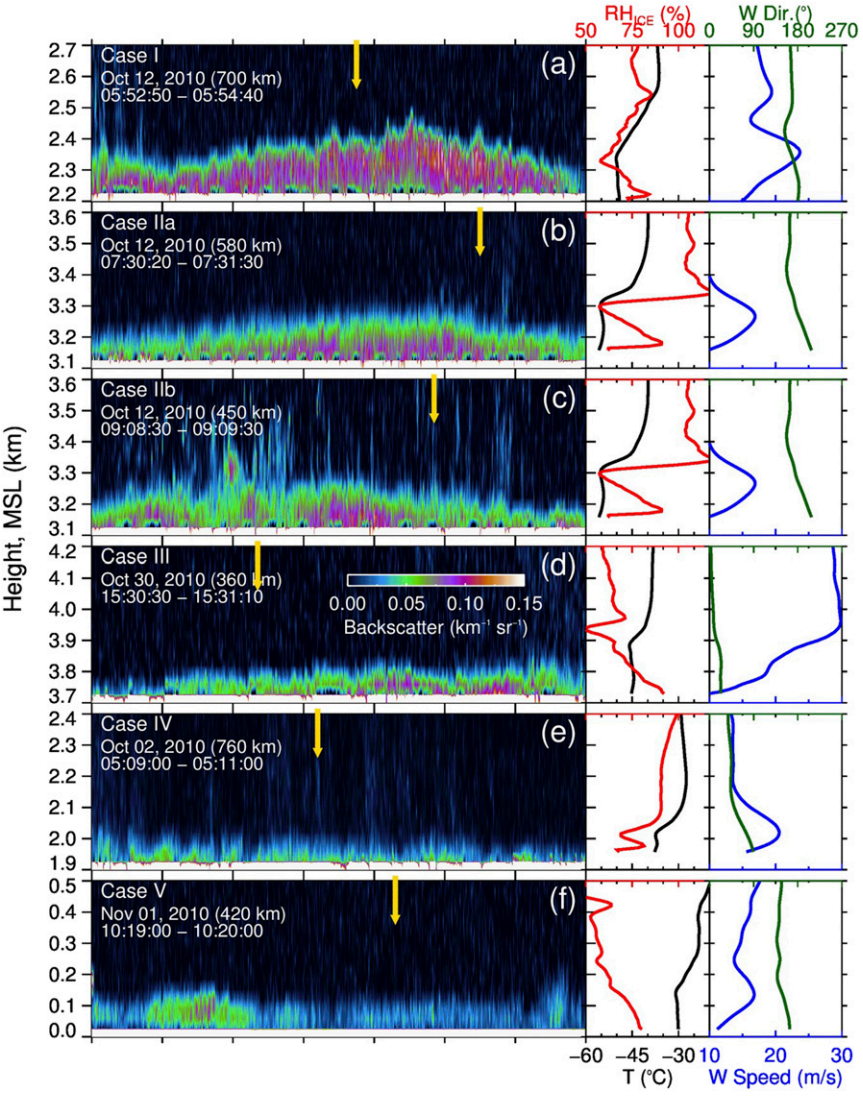

FIG. 4. (a)–(f) CALIOP 532-nm calibrated, attenuated backscatter along the *CALIPSO* tracks shown in Fig. 2 and the corresponding dropsonde temperature (black line), relative humidity with respect to ice (red line), wind speed (blue line), and wind direction (green line) for the five case studies. The vertical yellow arrow at the top of the images denotes the point along the *CALIPSO* track nearest to the dropsonde location. The height scale to the left of the image is with respect to mean sea level at the location of the dropsonde. Dropsonde locations and times are listed in Table 1.

descending katabatic flow. Following Stull (2009), we computed the gradient Richardson number [Eq. (2)] within the blowing-snow layer from the dropsonde data and obtained a value of 0.03, which indicates a high degree of turbulent mixing within the layer:

$$R = \frac{\dfrac{g}{\theta_v}\dfrac{\partial \overline{\theta}_v}{\partial z}}{\left[\left(\dfrac{\partial \overline{U}}{\partial z}\right)^2 + \left(\dfrac{\partial \overline{V}}{\partial z}\right)^2\right]}, \qquad (2)$$

where θ_v is the virtual potential temperature and $\overline{U}$ and $\overline{V}$ are the layer average zonal and meridional components of the wind speed, respectively.

Figure 8 shows AWS data from stations closest to the dropsonde locations. The top panel shows the temperature, relative humidity (with respect to ice), and wind speed from AWS station Irene (71.63°S, 148.67°E; the locations of the AWS stations are shown on the map in Fig. 2), which is 183 km to the east of the dropsonde location. The time of the dropsonde is indicated by the vertical gray-shaded bar (1242 UTC), and the time of the

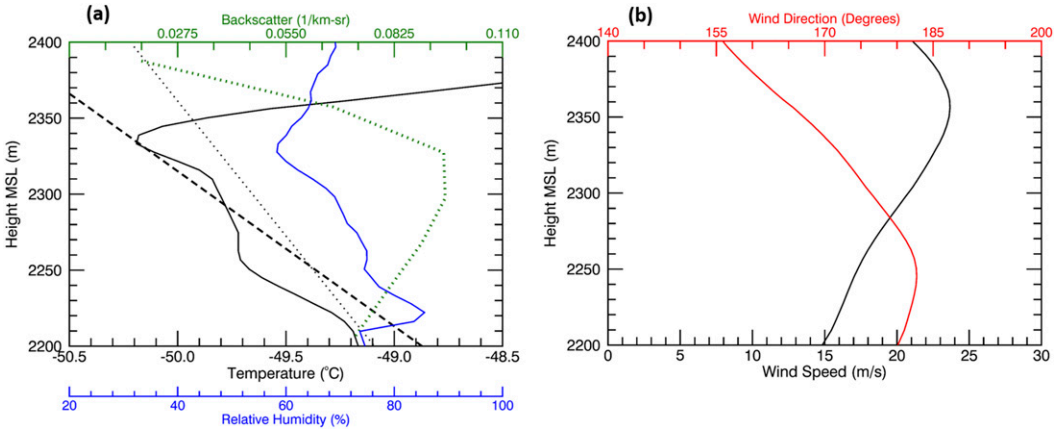

FIG. 5. (a) A magnified view of the dropsonde temperature (black solid line), humidity (blue solid line), and CALIOP average backscatter (green dotted line) profiles for case I. Also shown are the dry (black dashed line) and moist (black dotted line) adiabatic lapse rates. (b) Dropsonde wind speed (black) and direction (red) through the blowing-snow layer for case I.

CALIPSO track is shown by the blue bar. At the time of the dropsonde, the AWS temperature, relative humidity, and wind speed (−50°C, 72%, and 13 m s^{-1}) all agree well with the near-surface values measured by the dropsonde (−50°C, 75%, and 15 m s^{-1}). At the time of the *CALIPSO* track (0550 UTC) the AWS 3-m wind speed was considerably higher (18 m s^{-1}) and temperature and relative humidity were somewhat higher (−47.5°C and 79%, respectively).

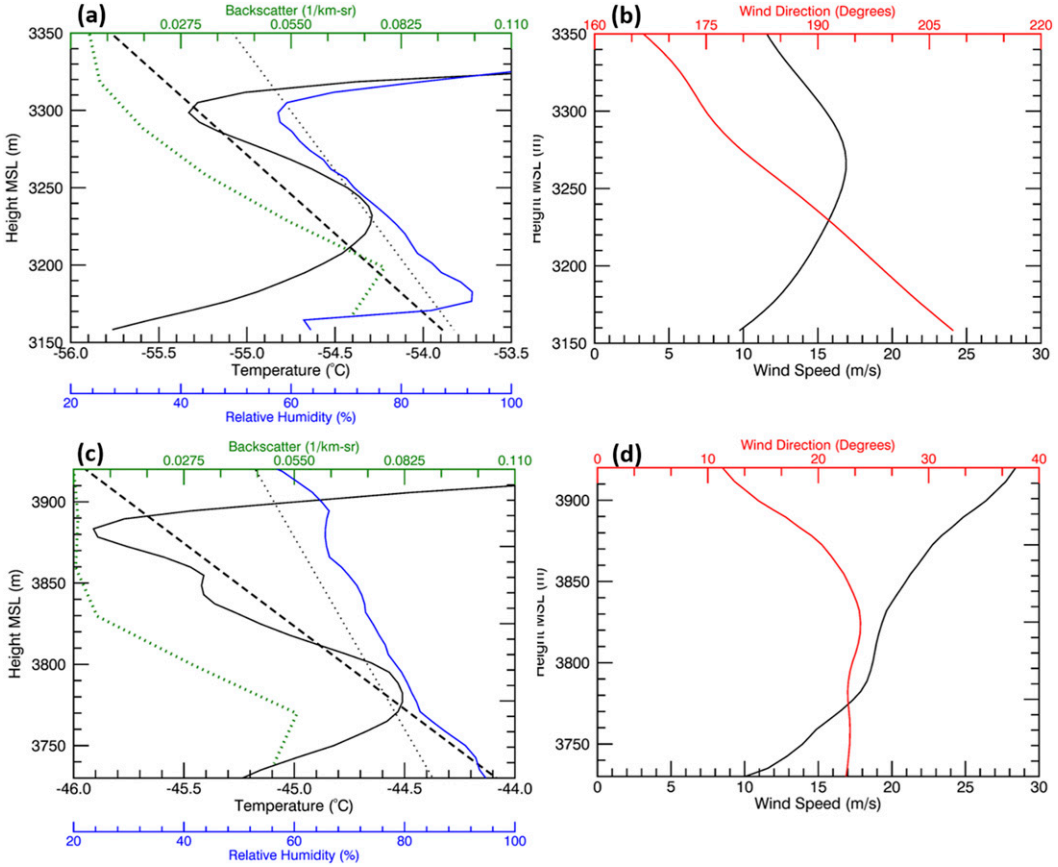

FIG. 6. (a) As in Fig. 5a, but for the dropsonde and CALIOP average backscatter of case II. (b) As in Fig. 5b, but for the dropsonde for case II. (c) As in Fig. 5a, but for case III. (d) As in Fig. 5b, but for case III.

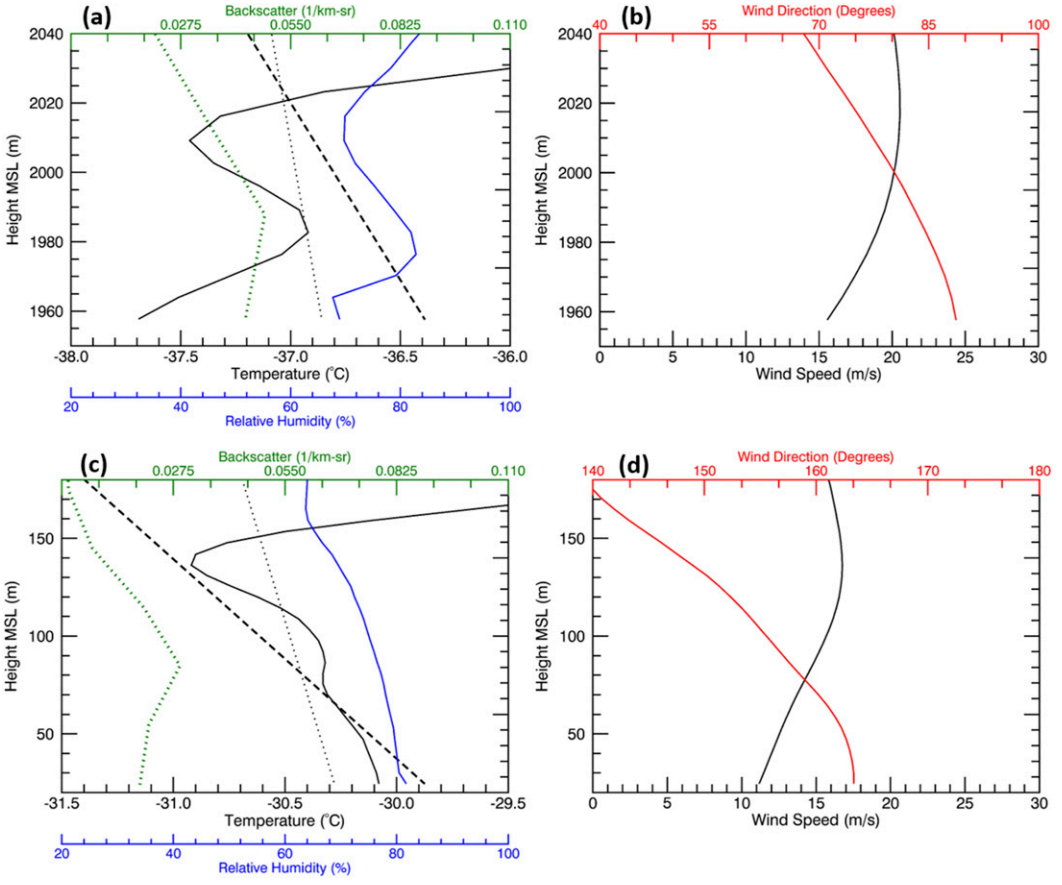

FIG. 7. (a) As in Fig. 5a, but for the dropsonde and CALIOP average backscatter of case IV. (b) As in Fig. 5b, but for the dropsonde for case IV. (c) As in Fig. 5a, but for case V. (d) As in Fig. 5b, but for case V.

b. *Case II*

Case II (shown in Figs. 4b,c and Figs. 6a,b) also occurred on 12 October 2010, but about 900 km southwest of case I. At this location, the surface elevation (3150 m) is much higher than that for case I and the temperature is much lower. The dropsonde was launched at 1049 UTC and reached the surface at 77.19°S, 121.09°E. There were two *CALIPSO* tracks that came within 150 and 200 km of the dropsonde a few hours prior to the dropsonde data. While this distance between the dropsonde and the *CALIPSO* data is large, we are confident that blowing snow was occurring at the location and time of the dropsonde, as evidenced by the MODIS data at 0550 UTC that indicated blowing snow was widespread in and around the position of the dropsonde (Fig. 3). Note also that there are a total of four *CALIPSO* tracks (yellow lines in Fig. 3) that surround the dropsonde location for which blowing snow was detected, one of which occurred after the time of the dropsonde. Figures 4b and 4c show the CALIOP backscatter from the two *CALIPSO* tracks that came nearest to the dropsonde at 0730 and 0908 UTC (red *CALIPSO* tracks for case II in Fig. 2). Blowing snow is plainly visible in the lower 100–150 m at the position of closest approach to the dropsonde (vertical yellow arrow in the images).

The temperature profile in Figs. 4b and Fig. 6a shows a small decrease as the dropsonde descends until it reaches about 3400 m MSL, at which point a sharp decrease begins (~10°C over just 100 m) and continues to the height of the top of the blowing-snow layer (~3300 m MSL). From that point downward to about 3250 m MSL, the temperature increases by about 1°C (moving downward). The lapse rate in the upper 60 m of the blowing-snow layer is 0.015°C m^{-1}, which is greater than dry adiabatic (0.0098°C m^{-1}). The surface temperature is approximately −56°C and would be much lower if the strong inversion had continued all the way to the surface.

The relative humidity profile (red line in Fig. 4b and blue line in Fig. 6a) is supersaturated (about 110%) above the blowing-snow layer and begins a sharp decrease at about 3350 m MSL. At roughly the height where the temperature profile begins to increase (moving downward), the relative

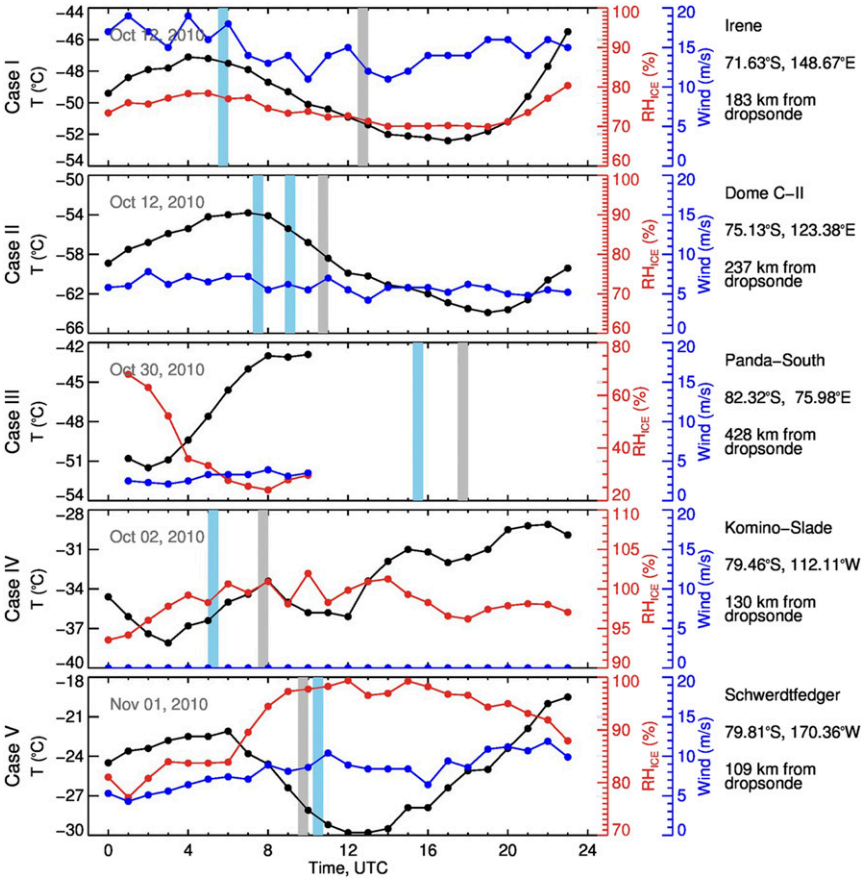

FIG. 8. AWS data for sites closest to the dropsonde locations for the dates of the five cases. Temperature, wind speed, and relative humidity with respect to ice are shown as the black, blue, and red lines, respectively. The blue vertical bars represent the times of the dropsondes, and the gray vertical bars are the times of the CALIOP backscatter data. The locations of the AWS stations are listed to the right of the graph and are also shown in Fig. 2.

humidity profile begins a sharp increase after reaching a minimum of about 60% very near the top of the blowing-snow layer. The relative humidity increases downward in a linear fashion and reaches a maximum of about 95% within about 25 m of the surface. From 25 m to the surface it decreases to about 80%.

The wind speed (blue line in Fig. 4b and black line in Fig. 6b) is about 10 m s^{-1} above the blowing-snow layer and increases sharply (as the dropsonde descends) near the top of the layer (3300 m MSL), reaching a maximum of 17 m s^{-1} just below the layer top (3275 m MSL). From this maximum, the wind speed decreases sharply, reaching a value of 10 m s^{-1} near the surface. The wind direction is from about 160° above the blowing-snow layer and begins changing direction at the same height as the wind speed increases. The wind direction changes from 160° to 205° over a vertical distance of 200 m (mostly through the depth of the blowing-snow layer). This is a large amount of directional wind shear which, combined with the wind speed sheer, will tend to produce mechanical mixing of the air. The Richardson number for this case was 0.10, which again indicates a high level of turbulence.

The closest AWS station (Dome C-II in Fig. 8) for this case was 237 km from the dropsonde location and did not have relative humidity data. The temperature near the surface at the time of the dropsonde (1049 UTC) was −58°C and close to the dropsonde value (−56°C). The AWS wind speed of 6 m s^{-1} is much lower than that measured by the dropsonde (10 m s^{-1}).

c. *Case III*

The third case (shown in Fig. 4d) occurred over the high East Antarctic plateau at 81°S, 50.5°E on 30 October 2010. Here the surface elevation is 3750 m and is a location that does not typically experience a high frequency of blowing snow (Palm et al. 2018). The left panel of Fig. 4d shows the CALIOP backscatter data

acquired at 1530:30–1531:10 UTC and taken along the *CALIPSO* track shown in Fig. 2. The blowing-snow layer as measured by CALIOP was about 100 m thick at the point nearest the dropsonde. Interestingly, the temperature and moisture profiles in Figs. 4d and 6c indicate a layer depth closer to 200 m. This could be due to the temporal or spatial difference between the two observations (2.5 h and 50 km, respectively).

The relative humidity profile shown in Figs. 4d and 6c is decidedly different than the previous case in that it shows a linear increase all the way to the surface. The relative humidity near the top of the blowing-snow layer is about 65% increasing to about 95% near the surface. Of the five cases presented here, this is the highest measured near-surface relative humidity.

The dropsonde wind speed (Figs. 4d and 6d) is very high above the blowing-snow layer (30 m s^{-1}) and begins an almost linear decrease at about 3950 MSL, which is very close to the height where the temperature profile becomes nearly dry adiabatic (and close to the height of the top of the blowing-snow layer). The wind speed continues to decrease downward and has a value near 10 m s^{-1} at the surface. The wind direction is fairly constant through the depth of the layer. Even so, there is a large amount of wind speed shear within the blowing-snow layer, which is conducive to the production of turbulence. The layer average Richardson number of −0.05 shows that, in addition to shear-generated instability, there is also convective instability in the layer. This is a result of the near superadiabatic lapse rate in the upper 100 m of the blowing-snow layer.

d. Case IV

Case IV (shown in Figs. 4e and 7a,b) is over central West Antarctica on 2 October 2010 near 79°S, 106°W. The CALIOP backscatter data shown in Fig. 4e were acquired at 0509–0511 UTC along a ground track that passed about 40 km to the northwest of the dropsonde. The time separation between the dropsonde and CALIOP data was about 2.5 h. As seen in Fig. 4e, the blowing-snow layer was very shallow, averaging about 75–100 m in thickness.

The temperature profile in Figs. 4e and 7a shows a strong inversion from about 2200 m MSL to near the top of the blowing-snow layer (2020 m MSL). At that height or slightly below, the temperature profile traces out an "S" pattern, where it initially begins to increase and then decreases. This same pattern can be seen in the temperature profile of case III within the blowing-snow layer. The temperature lapse rate is positive in the lower 30 m of the layer, but becomes negative up to 50 m and then positive again above that to the top of the layer (80 m). The dropsonde-measured surface temperature is −38°C and compares well to the ERA-5 2-m temperature in online supplemental Fig. S3a but is somewhat higher than the nearest AWS station at −34°C (Komino-Slade in Fig. 8)

The relative humidity profile in Fig. 7a is about 80% above the blowing-snow layer and then decreases to 70% near the top of the layer. The relative humidity then begins to increase slightly below the top of the blowing-snow layer (60 m), reaches 80% about 20 m above the surface, and then decreases to 70% at the ground. The corresponding ERA-5 2-m relative humidity shown in online supplemental Fig. S3b is about 85%–90% and the closest AWS station (Komino-Slade) relative humidity is near 100%.

The wind speed profile shown in Fig. 7b reaches a maximum of 21 m s^{-1} very near the top of the blowing-snow layer and then decreases to 16 m s^{-1} near the surface. The Richardson number for this case is 0.17 and, while larger than the other cases, still indicates a turbulent layer. It is interesting to note that the near-surface wind speed for this case is the highest of all of the cases and yet the blowing-snow layer is relatively shallow and the backscatter is fairly low. This may indicate that there are some characteristics of the snow, such as age, density, and temperature history, that make it harder to become airborne.

e. Case V

The last case we present (shown in Figs. 4f and 7c,d) occurred over the Ross Ice Shelf on 1 November 2010. This case was especially well collocated in space and time and is also the only case close to sea level. The time difference between the CALIOP data and the dropsonde was only 20 min and the two measurements were separated by just 12 km. Figure 4f shows the CALIOP backscatter data. The blowing-snow layer is about 100 m thick and has considerable variability in height and backscatter strength along the track. Another aspect of this case worth mentioning is that the air temperature near the surface was considerably higher than the other cases. As mentioned in section 3a, the relative humidity sensor on the Vaisala RS92 dropsonde has larger error and time lag as temperature decreases. With lower tropospheric temperature being between −20° and −30°C, this may mean that the moisture profile measured by the dropsonde is more accurate for this case.

The temperature profile in Fig. 4f shows the temperature inversion extending up to 300 m MSL and relatively warm air at 500 m (−20°C) above the surface and becoming lower as the dropsonde descends. At about 225 m above the surface the temperature decreases sharply (moving downward), indicating the characteristics of the typical near-surface inversion. As seen in Fig. 7c, at

TABLE 2. Air temperature (°C) at, and height (m MSL) of, the top and bottom of temperature inversion, inversion slope (°C m^{-1}), blowing-snow layer depth (m), relative humidity (%) with respect to ice at layer top and at the surface, maximum wind speed (m s^{-1}) within the blowing-snow layer, and the Richardson number for each of the five case studies.

Case	Temperature (height) at inversion bottom	Temperature (height) at inversion top	Inversion slope	Blowing-snow layer depth	Relative humidity at layer top/the surface	Max wind speed	Richardson no.
I	−51 (2350)	−37 (2600)	0.056	170	60/75	21	0.03
II	−56 (3300)	−40 (3500)	0.080	150	64/60	16	0.10
III	−50 (3900)	−40 (4000)	0.100	100	68/94	20	−0.05
IV	−38 (2050)	−27 (2150)	0.110	80	72/68	20	0.17
V	−31 (150)	−22 (250)	0.090	100	70/82	18	0.03

about 140 m above the surface, and again corresponding to the top of the blowing-snow layer, the lapse rate abruptly changes to slightly increasing as the dropsonde descends. The minimum temperature of −30.9°C occurs at 130 m above the surface while the near-surface temperature is −30.1°C. The temperature lapse rate through the blowing-snow layer of −0.0080°C m^{-1} is between moist and dry adiabatic.

The relative humidity profile in Fig. 4f shows relatively dry conditions at 500 m above the surface (<40%) and then a sharp humidity increase to around 60% at 400 m. From that height and as the dropsonde descends the relative humidity begins a steady increase that continues throughout the depth of the blowing-snow layer (Fig. 7c).

The wind profile shown in Fig. 7d shows a general decrease from 22 m s^{-1} near the blowing-snow layer top to about 11 m s^{-1} near the surface. The wind speed near the surface is about 11 m s^{-1}, which agrees well with the AWS value of 10 m s^{-1}. The wind direction veers from 135° at 200 m height to 162° at the surface. The near–dry adiabatic temperature profile in the blowing-snow layer combined with the wind shear produces a Richardson number of 0.03, again indicating strong turbulence.

5. Discussion

From the five blowing-snow cases presented above, it is apparent that during deep blowing-snow episodes the vertical temperature structure in the lowest few hundred meters does not show the typical strong inversion extending to the ground; instead, the lapse rate within the blowing-snow layer sometimes approaches or exceeds dry adiabatic. This usually occurs in the upper half of the blowing-snow layer. The average lapse rate for the depth of the layer is usually between moist and dry adiabatic. Above the blowing-snow layer the temperature profile retains the familiar inversion character and increases at a rate of about 5°–8°C per 100 m up to a height of typically 300–400 m above the surface. Also note that in all cases the surface temperature would be about 5°–10°C lower had the temperature inversion extended all the way to the surface. This indicates that the high wind speed and shear (speed and direction) present during deep blowing-snow events produce turbulence and promote mixing of the warmer air aloft, which raises the temperature at the surface. The surface temperature increases even though sublimation of snow particles will tend to lower the temperature. It is also important to note that the dropsonde data for all five cases shown here were acquired at night. Insolation, even over a snow-covered surface, can cause a near–dry adiabatic temperature lapse rate in the lowest 100–200 m of the boundary layer (Sorbjan et al. 1986).

The blowing snow is confined to the near-isothermal shallow layer as buoyancy forces restrict the air, containing it from penetrating into the stable layer aloft. The case studies indicated that the depth of the blowing-snow layer was not related to near-surface wind speed but did seem to be correlated with the strength of the overlying inversion (Table 2). The Richardson number for all cases was considerably below the threshold value considered to demarcate a turbulent layer (0.25). Only case III exhibited a negative Richardson number, indicating convective instability combined with wind-shear-induced turbulence.

The results also raise the following questions: does the observed temperature structure have anything to do with the blowing snow itself? Or is it merely the result of high wind speeds and wind shear causing turbulence, which mixes the warmer air down to lower levels, destroying the inversion near the surface? In certain areas the same temperature structure can be the result of downslope flow warming the air adiabatically, as is known to occur in the katabatic wind regime (Bromwich 1989) or a combination of the two processes (mixing from above and downslope warming). However, case V presented above occurred over the Ross Ice Shelf, the flow over which is not downslope. Thus, it appears that wind-shear-induced turbulent mixing plays a large role here. It is possible that blowing-snow particles within the layer have an effect on the temperature structure

through cooling by sublimation and also warming by the absorption of longwave radiation. The best way to answer this question is to find a dropsonde that shows high winds in an area where blowing snow is not occurring. This is difficult because snow is almost always available over most of Antarctica. Possible exceptions are the areas where wind has scoured all snow away (Das et al. 2013). However, we were not able to find examples of dropsondes close to *CALIPSO* tracks for which there were high winds and no blowing snow. There are numerous dropsondes with temperature inversions extending to the ground and all of those have relatively light winds and are not aligned temporally and spatially with *CALIPSO* tracks. Thus, for these cases, we were not able to ascertain definitively whether blowing snow was present.

The moisture profiles obtained by the dropsondes showed that the relative humidity was highest close to the surface (normally about 80%–90%) and decreased with height through the depth of the blowing-snow layer. This observation is consistent with the hypothesis that wind-shear-driven turbulence is entraining warmer and lower relative humidity air from the inversion above, thereby keeping the upper portion of the blowing-snow layer from reaching saturation even in the presence of sublimation. However, the uncertainty in the relative humidity measurements in extremely cold environments is considerable. The results of Miloshevich et al. (2009) indicate that the moisture measurements may have a negative bias of 10%–15%. Even so, adding 15% to the relative humidity would still leave much of the upper portion of the blowing-snow layer below saturation. The highest relative humidity recorded within the blowing-snow layer for the five cases was 95% (near the surface) for case III. However, even for this case the dropsonde data/measurements suggest/indicate that the humidity fell precipitously, higher up in the blowing-snow layer.

The surface wind speed for the five cases averaged $12\,\mathrm{m\,s^{-1}}$ and always increased with height through the depth of the blowing-snow layer, reaching a maximum at or very near the top of the layer (usually near $20\,\mathrm{m\,s^{-1}}$). Above that height, the wind speed decreased sharply for all but case III. A high degree of directional wind shear was present (in four of the five cases) through the depth of the blowing-snow layer, usually changing by 25°–30° in direction over just 200 m. These changes in wind velocity will produce turbulence and promote mixing throughout the layer.

These observations give at least some support to the hypothesis put forth in section 2, namely, that the high wind speed and wind shear seemingly always present in deep blowing-snow layers produce turbulent mixing of the overlying inversion, entraining warmer and lower relative humidity air into the blowing-snow layer. This mixing process produces a near-isothermal (sometimes even approaching or exceeding dry adiabatic) temperature profile within the blowing-snow layer and acts to keep the relative humidity below saturation for most of the depth of the layer.

6. Summary and conclusions

Drifting- and blowing-snow processes are well understood from the perspective of ground measurements. However, because of the scarcity of observations and the harsh conditions present in blowing-snow storms, little is known about the thermodynamic structure of fully developed, deep (>50 m) blowing-snow layers that cover large areas of Antarctica over 70% of the time in winter (April–October). As part of the Concordiasi project, 648 dropsondes were launched from numerous stratospheric balloons, providing profiles of temperature, moisture, and winds through the depth of the lower stratosphere and entire troposphere over most areas of Antarctica. Some of these dropsondes (28 in all) fell through or very near to deep blowing-snow layers, providing, for the first time, measurements of the thermodynamic structure of these layers. Five such cases were presented here showing that the temperature structure within the blowing-snow layer is constant or even decreasing with height, sometimes approaching dry adiabatic. Because the dropsonde data from all five cases were acquired at night, the observed temperature structure in the blowing-snow layer was in no way related to solar heating of the surface. This suggests that strong mixing in the layer, most likely the result of the observed large wind speed and directional wind shear, was responsible for the nearly well-mixed temperature structure. The lapse rate above the blowing-snow layers was always strongly stable (an inversion). The blowing-snow layer top as derived from *CALIPSO* backscatter data nearly always coincided with the bottom of the overlying temperature inversion. The relative humidity profile was always maximum near the surface or slightly above but never reached saturation. For most of the cases the dropsonde-measured relative humidity was 80%–90% near the surface, but one case (case III) did show relative humidity approaching 100% at the surface. However, even for this case the dropsonde measurements/data suggest/indicate that the humidity decreased sharply with increasing height through the depth of the blowing-snow layer.

It is noted that the Vaisala RS92 moisture sensor has difficulty measuring humidity accurately in very cold conditions and has a negative (dry) bias that depends on temperature (Miloshevich et al. 2006, 2009). Some of the

data presented here were acquired at temperatures between −50° and −60°C, for which the magnitude of the dry bias is likely between 10% and 15%. For the five cases presented here, the relative humidity near the surface exceeded 85% in only one case, and thus it can be concluded that in four of the five cases saturation was not reached. In general, relative humidity was greater in the lower 20–30 m of the blowing-snow layer, with the upper portion of the layer often in the 60%–75% range. Further evidence of a subsaturated layer comes from the temperature lapse rate, which was often near dry adiabatic in the upper half of the layer. If the air were saturated, the temperature lapse rate would follow moist adiabatic. These results have potentially important implications for the amount of water vapor that is sublimated into the atmosphere during blowing-snow storms and also for ice-sheet mass balance. We suggest future work should include the *CALIPSO* and dropsonde observations with the use of a blowing-snow-resolving model such as Modele Atmospherique Regional (MAR; Gallée et al. 2013) or the Antarctic ice sheet regional atmospheric climate model (RACMO2.1/ANT; Lenaerts et al. 2012) to better understand the blowing-snow processes and the model parameterizations used to describe them. In addition, a targeted field campaign that includes an aircraft equipped with a down-looking lidar and a dropsonde system would provide invaluable data to help to better understand blowing-snow layer dynamics. It is hoped that further work, both observational and modeling, will lead to more-definitive conclusions on the moisture structure within these blowing-snow layers that are pervasive if not ubiquitous over most of Antarctica.

Acknowledgments. This research was performed under NASA contracts NNH14CK40C and NNH14CK39C. The authors thank Thomas Wagner and David Considine for their support and encouragement. We also thank Mr. Alec Stiller for providing help with some figures. The *CALIPSO* data used in this study were obtained online from the NASA Langley Research Center Atmospheric Science Data Center (https://doi.org/10.5067/CALIOP/CALIPSO/CAL_LID_L1-STANDARD-V4-00_L1B-004.00). The dropsonde data were provided online by the NCAR Earth Observing Laboratory under the sponsorship of the National Science Foundation (https://data.eol.ucar.edu/dataset/221.002). ERA-5 data were obtained from the Meteorological Archival and Retrieval System (MARS) through the ECMWF's Web-API (more details are available at http://apps.ecmwf.int/datasets/). Blowing-snow data are available from the author and will soon be made available from the NASA Langley Research Center Atmospheric Science Data Center. The AWS data (except station Irene) are publicly available online (https://amrc.ssec.wisc.edu/). The data for AWS station Irene are also available online (http://www.climantartide.it/).

REFERENCES

Bintanja, R., 1998: The interaction between drifting snow and atmospheric turbulence. *Ann. Glaciol.*, **26**, 167–173, https://doi.org/10.1017/S0260305500014750.

——, 2000: Snowdrift suspension and atmospheric turbulence. Part II: Results of model simulations. *Bound.-Layer Meteor.*, **95**, 369–395, https://doi.org/10.1023/A:1002643921326.

——, 2001: Modelling snowdrift sublimation and its effect on the moisture budget of the atmospheric boundary layer. *Tellus*, **53A**, 215–232, https://doi.org/10.3402/tellusa.v53i2.12189.

Boylan, P., J. Wang, S. A. Cohn, T. Hultberg, and T. August, 2016: Identification and intercomparison of surface-based inversions over Antarctica from IASI, ERA-Interim, and Concordiasi dropsonde data. *J. Geophys. Res. Atmos.*, **121**, 9089–9104, https://doi.org/10.1002/2015JD024724.

Bromwich, D. H., 1989: Satellite analyses of Antarctic katabatic wind behavior. *Bull. Amer. Meteor. Soc.*, **70**, 738–749, https://doi.org/10.1175/1520-0477(1989)070<0738:SAOAKW>2.0.CO;2.

Das, I., and Coauthors, 2013: Influence of persistent wind scour on the surface mass balance of Antarctica. *Nat. Geosci.*, **6**, 367–371, https://doi.org/10.1038/ngeo1766.

Déry, S. J., and M. K. Yau, 1999: A bulk blowing snow model. *Bound.-Layer Meteor.*, **93**, 237–251, https://doi.org/10.1023/A:1002065615856.

——, P. A. Taylor, and J. Xiao, 1998: The thermodynamic effects of sublimating, blowing snow in the atmospheric boundary layer. *Bound.-Layer Meteor.*, **89**, 251–283, https://doi.org/10.1023/A:1001712111718.

Frezzotti, M., C. Scarchilli, S. Becagli, M. Proposito, and S. Urbini, 2013: A synthesis of the Antarctic surface mass balance during the last 800 yr. *Cryosphere*, **7**, 303–319, http://doi.org/10.5194/tc-7-303-2013.

Gallée, H., G. Guyomarc'h, and E. Brun, 2001: Impact of snow drift on the Antarctic ice sheet surface mass balance: Possible sensitivity to snow-surface properties. *Bound.-Layer Meteor.*, **99**, 1–19, https://doi.org/10.1023/A:1018776422809.

——, A. Trouvilliez, C. Agosta, C. Genthon, V. Favier, and F. Naaim-Bouvet, 2013: Transport of snow by the wind: A comparison between observations in Adélie Land, Antarctica, and simulations made with the regional climate model MAR. *Bound.-Layer Meteor.*, **146**, 133–147, https://doi.org/10.1007/s10546-012-9764-z.

Grazioli, J., J. Madeleine, H. Gallée, R. M. Forbes, C. Genthon, G. Krinner, and A. Bernea, 2017: Katabatic winds diminish precipitation contribution to the Antarctic ice mass balance. *Proc. Natl. Acad. Sci. USA*, **114**, 10 858–10 863, https://doi.org/10.1073/pnas.1707633114.

Hersbach, H., and D. Dee, 2016: ERA5 reanalysis is in production. *ECMWF Newsletter*, No. 147, ECMWF, Reading, United Kingdom, 7, www.ecmwf.int/sites/default/files/elibrary/2016/16299-newsletter-no147-spring-2016.pdf.

King, J. C., and J. Turner, 1997: *Antarctic Meteorology and Climatology*. Cambridge University Press, 424 pp.

Kodama, Y., G. Wendler, and J. Gosink, 1985: The effect of blowing snow on katabatic winds in Antarctica. *Ann. Glaciol.*, **6**, 59–62, https://doi.org/10.1017/S026030550000999X.

Lenaerts, J. T. M., M. R. van den Broeke, S. J. Déry, E. van Meijgaard, W. J. van de Berg, S. P. Palm, and J. Sanz Rodrigo, 2012: Modeling drifting snow in Antarctica with a regional climate model: 1. Methods and model evaluation. *J. Geophys. Res.*, **117**, D05108, https://doi.org/10.1029/2011JD016145.

Mahesh, A., R. Eager, J. R. Campbell, and J. D. Spinhirne, 2003: Observations of blowing snow at the South Pole. *J. Geophys. Res.*, **108**, 4707, https://doi.org/10.1029/2002JD003327.

Mann, G. W., P. S. Anderson, and S. D. Mobbs, 2000: Profile measurements of blowing snow at Halley, Antarctica. *J. Geophys. Res.*, **105**, 24 491–24 508, https://doi.org/10.1029/2000JD900247.

Miloshevich, L. M., A. Paukkunen, H. Vomel, and S. J. Oltmans, 2004: Development and validation of a time-lag correction for Vaisala radiosonde humidity measurements. *J. Atmos. Oceanic Technol.*, **21**, 1305–1327, https://doi.org/10.1175/1520-0426(2004)021<1305:DAVOAT>2.0.CO;2.

——, H. Vömel, D. N. Whiteman, B. M. Lesht, F. J. Schmidlin, and F. Russo, 2006: Absolute accuracy of water vapor measurements from six operational radiosonde types launched during AWEX-G and implications for AIRS validation. *J. Geophys. Res.*, **111**, D09S10, https://doi.org/10.1029/2005JD006083.

——, ——, ——, and T. Leblanc, 2009: Accuracy assessment and correction of Vaisala RS92 radiosonde water vapor measurements. *J. Geophys. Res.*, **114**, D11305, https://doi.org/10.1029/2008JD011565.

Nash, J., T. Oakley, H. Vömel, and W. Li, 2011: WMO intercomparisons of high quality radiosonde systems. WMO/TD-1580, Instruments and Observing Methods Rep. 107, 248 pp., https://www.wmo.int/pages/prog/www/IMOP/publications/IOM-107_Yangjiang.pdf.

Ohata, T., S. Kobayashi, N. Ishikawa, and S. Kawaguchi, 1985: Structure of the katabatic winds at Mizuho Station, East Antarctic. *J. Geophys. Res.*, **90**, 10 651–10 658, https://doi.org/10.1029/JD090iD06p10651.

Palm, S. P., Y. Yang, J. D. Spinhirne, and A. Marshak, 2011: Satellite remote sensing of blowing snow properties over Antarctica. *J. Geophys. Res.*, **116**, D16123, https://doi.org/10.1029/2011JD015828.

——, V. Kayetha, Y. Yang, and R. Pauly, 2017: Blowing snow sublimation and transport over Antarctica from 11 years of CALIPSO observations. *Cryosphere*, **11**, 2555–2569, https://doi.org/10.5194/tc-11-2555-2017.

——, —— and ——, 2018: Toward a satellite-derived climatology of blowing snow over Antarctica. *J. Geophys. Res. Atmos.*, **123**, 10 301–10 313, https://doi.org/10.1029/2018JD028632.

Phillpot, H. R., and J. W. Zillman, 1970: The surface temperature inversion over the Antarctic continent. *J. Geophys. Res.*, **75**, 4161–4169, https://doi.org/10.1029/JC075i021p04161.

Rabier, F., and Coauthors, 2010: The Concordiasi project in Antarctica. *Bull. Amer. Meteor. Soc.*, **91**, 69–86, https://doi.org/10.1175/2009BAMS2764.1.

——, and Coauthors, 2013: The Concordiasi field experiment over Antarctica: First results from innovative atmospheric measurements. *Bull. Amer. Meteor. Soc.*, **94**, ES17–ES20, https://doi.org/10.1175/BAMS-D-12-00005.1.

Rogers, R. R., and M. K. Yau, 1989: *A Short Course in Cloud Physics*. 3rd ed. Pergamon, 293 pp.

Scarchilli, C., M. Frezzotti, P. Grigioni, L. De Silvestri, L. Agnoletto, and S. Dolci, 2010: Extraordinary blowing snow transport events in East Antarctica. *Climate Dyn.*, **34**, 1195–1206, http://doi.org/10.1007/s00382-009-0601-0.

Sorbjan, Z., Y. Kodama, and G. Wendler, 1986: Observational study of the atmospheric boundary layer over Antarctica. *J. Climate Appl. Meteor.*, **25**, 641–651, https://doi.org/10.1175/1520-0450(1986)025<0641:OSOTAB>2.0.CO;2.

Stearns, C. R., and G. Wendler, 1988: Research results from Antarctic automatic weather stations. *Rev. Geophys.*, **26**, 45–61, https://doi.org/10.1029/RG026i001p00045.

Stull, R. B., 2009: *An Introduction to Boundary Layer Meteorology*. Springer, 670 pp.

Tabler, R. D., 1975: Estimating the transport and evaporation of blowing snow. Snow Management on the Great Plains, Great Plains Agricultural Council Publ. 73, University of Nebraska, 85–105.

Takahashi, S., 1985: Characteristics of drifting snow at Mizuho station, Antarctica. *Ann. Glaciol.*, **6**, 71–75, https://doi.org/10.1017/S0260305500010028.

Tomasi, C., and Coauthors, 2006: Characterization of the atmospheric temperature and moisture conditions above Dome C (Antarctica) during austral summer and fall months. *J. Geophys. Res.*, **111**, D20305, http://doi.org/10.1029/2005JD006976.

Vaisala, 2013: Vaisala radiosonde RS92-SGP data sheet. Vaisala, Inc., https://www.vaisala.com/sites/default/files/documents/RS92SGP-Datasheet-B210358EN-F-LOW.pdf.

Wamser, G., and V. Lykossov, 1995: On the friction velocity during blowing snow. *Contrib. Atmos. Phys.*, **68** (1), 85–94.

Wang, J., T. Hock, S. A. Cohn, C. Martin, N. Potts, T. Reale, B. Sun, and F. Tilley, 2013: Unprecedented upper-air dropsonde observations over Antarctica from the 2010 Concordiasi Experiment: Validation of satellite-retrieved temperature profiles. *Geophys. Res. Lett.*, **40**, 1231–1236, https://doi.org/10.1002/grl.50246.

Winker, D. M., M. A. Vaughan, A. Omar, Y. Hu, K. A. Powell, Z. Liu, W. H. Hunt, and S. A. Young, 2009: Overview of the CALIPSO mission and CALIOP data processing algorithms. *J. Atmos. Oceanic Technol.*, **26**, 2310–2323, https://doi.org/10.1175/2009JTECHA1281.1.

Yang, Y., S. P. Palm, A. Marshak, H. Yu, and Q. Fu, 2014: First satellite detected perturbations of outgoing longwave radiation associated with blowing snow events over Antarctica. *Geophys. Res. Lett.*, **41**, 730–735, https://doi.org/10.1002/2013GL058932.